ELSEVIER

Marine Geology 236 (2007) 189–208

MARINE GEOLOGY
INTERNATIONAL JOURNAL OF MARINE GEOLOGY, GEOCHEMISTRY AND GEOPHYSICS

www.elsevier.com/locate/margeo

Comparing the smooth, parabolic shapes of interfluves in continental slopes to predictions of diffusion transport models

Neil C. Mitchell [a,*], John M. Huthnance [b]

[a] *School of Earth, Ocean and Planetary Sciences, Cardiff University, Cardiff, UK*
[b] *Proudman Oceanographic Laboratory, Joseph Proudman building, 6 Brownlow Street, Liverpool L3 5DA, UK*

Received 24 March 2005; received in revised form 17 October 2006; accepted 20 October 2006

Abstract

Computer models of stratigraphic development at continental margins often include elements in which sediment topography evolves according to a diffusion equation, representing effects of down-slope sediment transport. However, there has been little effort to verify the model, for example by showing whether deposit geometries are as expected from it or by considering whether transport is consistent with the model's assumptions. The issue is important for understanding transport, erosion and deposition in continental slopes more generally and the extent to which such processes are recorded in seabed morphology. Examples of slope topography illustrating diffusive-like characteristics are examined here. In the uppermost slope of the USA central Atlantic margin, sandy areas between canyon heads are smoothly convex-upwards and almost parabolic, a morphology similar to subaerial soil-mantled hillslopes known to evolve according to a diffusion equation. Other data of interfluves in muddy sediment from both Atlantic and Pacific USA margins also show this smooth convex-upwards form.

In subaerial hill crests, the upwards-convex parabolic shape arises where steady erosion by streams along channels provide constant flux boundary conditions (i.e., the parabola is the steady-state solution to the diffusion equation). Although submarine processes will likely be different, the similar morphology of submarine interfluves prompts the question as to whether erosion along channels and movements of sediment between channels can also sometimes occur to cause a diffusive-like evolution of topography. The discussion therefore focuses on submarine processes affecting erosion and deposition, in particular to address whether the morphology results from true diffusion (which requires that sediment moves down-slope with a transport flux proportional to local bed gradient) or is fortuitous (sediment transport is instead unrelated to local bed gradient and the morphology arises from other effects on accumulation rates).

Keywords: diffusion sediment transport model; bedload transport; sediment creep; continental slope morphology; multibeam echosounder data

1. Introduction

Some seabed morphology is curiously similar to soil-mantled lowland landscapes, where the topography of hillslopes is often modelled with diffusion equations (e.g., Culling, 1963; Kirkby, 1971; Tucker and Bras, 1998; Dietrich et al., 2003). In such models, soil movements caused by creep, rainsplash and biological activity occur

* Corresponding author. Now at: School of Earth, Atmospheric and Environmental Sciences, the University of Manchester, Oxford Road, Manchester, UK. Tel.: +44 2920 875051; fax: +44 2920 874026.
E-mail address: neil@ocean.cf.ac.uk (N.C. Mitchell).

0025-3227/$ - see front matter
doi:10.1016/j.margeo.2006.10.028

with fluxes nearly proportional to the soil gradient. When conservation of mass is taken into account (convergence of soil flux implies deposition and divergence implies erosion), soil topography is predicted to evolve according to a diffusion equation, as will be shown later.

If the diffusion transport model were to apply in submarine settings, knowing where it applies could be useful for understanding how submarine landscapes develop and for developing realistic simulations of stratigraphy. Kenyon and Turcotte (1985) argued that sediment in shallow water can creep from surface wave loading and bioturbation, at rates proportional to bed gradient, as required by the model. They showed that the exponential shapes of delta fronts replicate steady-state solutions to the diffusion equation with constant river input of sediment as a boundary condition. Goff (2001) speculated that the smooth, upwards-convex morphology of the Hudson Apron (New Jersey slope) was caused by creep. Diffusion equations have also been used to represent redistribution of sediment on delta fronts (Syvitski et al., 1988; Syvitski and Daughney, 1992).

Many large-scale stratigraphic models have used diffusion equations to represent effects of marine sediment transport (Jordan and Flemings, 1991; Wolfe et al., 1994; Flemings and Grotzinger, 1997; Driscoll and Karner, 1999; Granjeon and Joseph, 1999; Penn and Harbaugh, 1999; Quiquerez et al., 2004). Some simulations have included a diffusion mobility parameter decreasing with water depth to represent decreasing agitation of the seabed by surface waves, which reproduce rounded clinoform rollovers (Kaufman et al., 1991; Rivenaes, 1992; Syvitski and Daughney, 1992; Flemings and Grotzinger, 1997; Rivenaes, 1997; Schlager and Adams, 2001). Others incorporated diffusion of suspended sediment concentration (Clarke et al., 1983; Niedoroda et al., 1995; Carey et al., 1999), representing dispersal of suspensions produced by storm waves. As sediment concentrations produced during storms are largest in shallow water because of the proximity of waves, dispersal leads to sediment moving to deeper water and hence smoothes topography, which is characteristic of diffusion. Such mechanisms may explain how deposition is enhanced over active synclines relative to anticlines on the Eel River shelf (Spinelli and Field, 2003), and apparently damped topography (Goff et al., 1999). Simulations using the diffusion equation to represent sediment redistribution on the Mid-Atlantic Ridge also appear realistic (Webb and Jordan, 1993, 2001a,b). Despite the extensive use of the diffusion equation, however, it is unclear from these studies if seabed topography does follow a diffusion equation or if the model results mimic seabed topography only fortuitously.

This paper proceeds by showing some representative bathymetry and stratigraphy (Figs. 1–5) in which areas between channels are smoothly upwards-convex and almost parabolic. The origins of this morphology are then discussed in terms of processes leading to true diffusion and others leading fortuitously to diffusive-like geometry. Using seismic reflection data from northern California and the Atlantic USA margin, we compare sediment morphology with solutions to the diffusion equation, an approach used previously for other sedimentary environments (Mitchell, 1995, 1996).

2. Observations

Examples from the USA Atlantic and Pacific slopes illustrate two contrasting geological and oceanographic environments (Pietrafesa, 1983) where smooth parabolic interfluves occur. The Atlantic shelf edge is remote from modern sources of continentally derived sediment because of the wide shelf and strong along-slope currents, and currents in the uppermost slope are capable of mobilising sand (Csanady et al., 1988). In contrast, because of its generally narrow shelf and proximity of actively uplifting and eroding mountains, the shelf and slope of the Pacific margin typically receives large quantities of mud. Modern currents are smaller than in the Atlantic uppermost slope. Measurements made immediately south of the Fig. 3 area, for example, show weak tidally-averaged slope-parallel currents associated with the California Undercurrent (Ramp and Abbott, 1998; Collins et al., 2000). The Eel River area (Fig. 5) is a muddy environment with generally slow currents (Alexander and Simoneau, 1999), though peak flows associated with internal waves exceed 20 cm/s, resuspending silt (Cacchione et al., 2002).

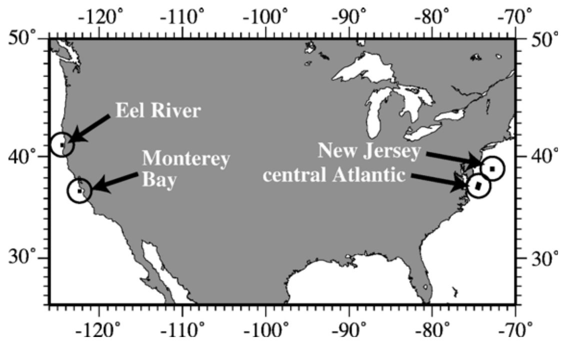

Fig. 1. Continental slope locations of the multibeam sonar datasets in Figs. 2–5.

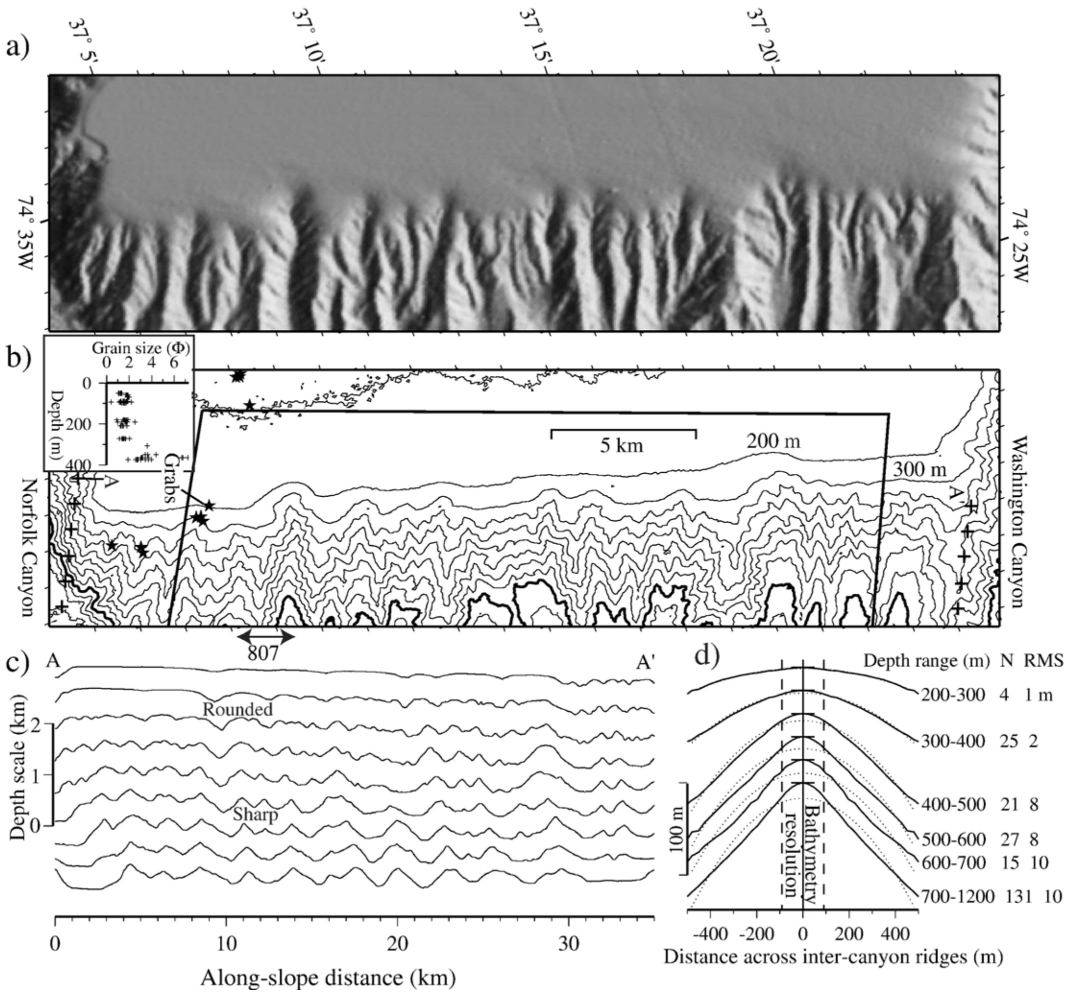

Fig. 2. The uppermost continental slope of the central Atlantic USA margin off Virginia. These morphologic data were originally collected with multibeam echo-sounders by the National Ocean Service and processed and gridded at 3″ resolution (~90 m) at the National Geophysical Data Center (Coastal Relief Model). (a) Shaded relief image of the data plotted in a transverse Mercator projection (artificial sun to the north). (b) Contours shown every 100 m with the 1000 m contour in bold. The plus symbols ('+') mark the ends of the cross-sections shown in (c). The outlined area marks the extent of data used to calculate gradients and curvatures for Fig. 6. The solid star symbols are locations of grab samples used to produce the grain-size graph shown in the inset (median values of ϕ for all grain-size measurements where $\phi = -\log_2$ (grain size(mm)); data from NOAA). Annotation "A807" and associated double-headed arrow mark the area of ALVIN dive 807 (Malahoff et al., 1982). (c) Along-slope topographic sections A–A' etc in (a). Vertical exaggeration is 2:1. (d) Average shapes of inter-canyon divides (interfluves) constructed by segmenting the data in (c) between maxima and minima points along each profile, offsetting each segment to the local maxima (interfluve crest) and then averaging all segments longer than 500 m (N = number of segments averaged). This average profile was then mirrored about the vertical axis to yield characteristic interfluve shapes. Dotted quadratic curves fitted by least-squares to the data show poor fits to the data below 400 m depth but reasonable fits shallower than 400 m. (RMS (root-mean-square) misfit values are given to the right of each graph.)

As is often the case in poorly accessible marine environments, we lack extensive stratigraphic and environmental information, so it is not strictly possible to assess in detail the extent to which seabed morphology is a result of modern conditions or is a relic of different conditions of the past, such as during the Last Glacial Maximum (LGM). Nevertheless, modern conditions (currents, biology, sediment texture) provide a starting point for discussion and some differences with earlier conditions can be anticipated. The length-scale of interest should be defined; surfaces can be smooth as expected from diffusion at a large scale but rough at smaller scales, e.g., rounded sandbanks covered by dunes. Conversely, some processes smooth surfaces at small scale but increase relief at large scale, e.g., contourite drifts generated by geostrophic currents. In this paper, we concentrate on morphology at intermediate-scale (>100 m) commensurate with the resolution of the

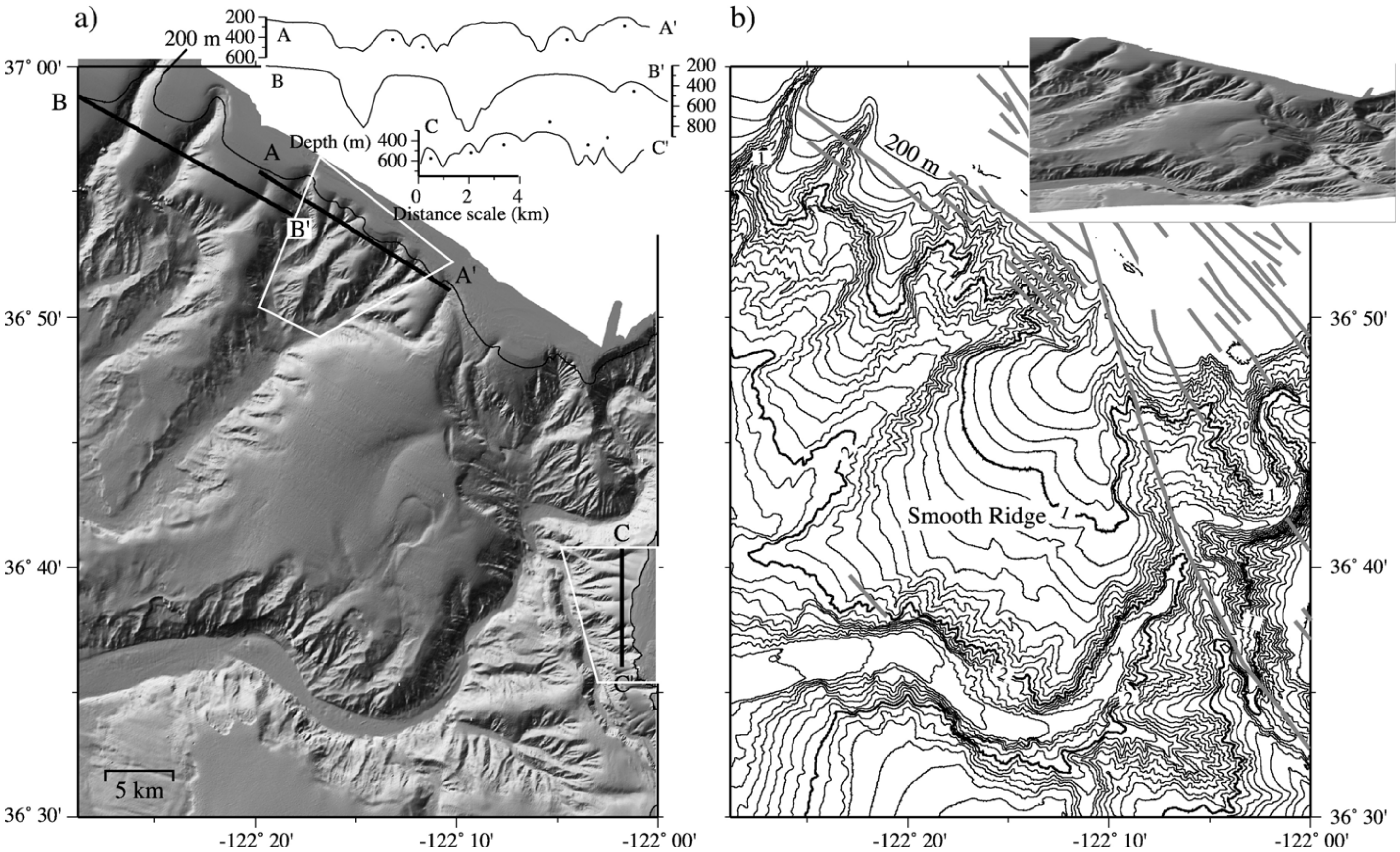

Fig. 3. (a) Shaded relief image of the Californian continental slope in Monterey Bay (Greene et al., 2002). A–A', etc mark the cross-sections in inset showing smooth upper walls around channels. White-outlined polygons show extents of data used to compute bed gradients and curvatures for Fig. 6a and b. (b) Map of depth contours shown every 100 m with 1000 m contours shown bold and annotated in km. Inset shows a 3D view of the shaded bathymetry in (a) from the south. The bathymetry data were collected by Monterey Bay Aquarium Research Institute scientists with a Simrad EM300 multibeam sonar on *R/V Ocean Alert* and provided as a 25 m grid (MBARI Mapping Team, 2000).

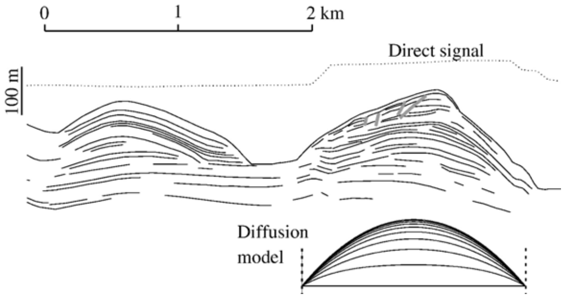

Fig. 4. Interpretation of stratigraphy in a high-resolution seismic profile collected along the New Jersey slope with a sparker seismic source and deeply towed hydrophone (Robb et al., 1981b). Depth scale represents water column; no allowance has been made for seismic velocity in sediments. Ridge crest lies at approximately 900 m depth. The curves (lower-right) represent aggradation within interfluves if transport were to be represented by a diffusion equation with constant elevation boundary conditions (at dashed lines) representing non-deposition along channels.

sonar data described. Given the lack of detailed stratigraphic control, the timescales over which surfaces acquired their shapes are also poorly known. A formal definition of “smoothness” is therefore omitted because the significance of particular relief is difficult to assess (a sharp step can persist because it was created recently or because of slow accumulation and/or erosion rates). Instead we simply identify smooth topography visually.

2.1. Atlantic multibeam sonar data

Fig. 2 shows the outermost continental shelf and upper slope of the central Atlantic USA. Interfluves within the slope are sharp, but shallower than 400 m they are generally rounded, which is emphasized by the cross-sections in Fig. 2c (drawn along the slope, A–A’ in Fig. 2b). Fig. 2d shows the characteristic shapes of the interfluves, sorted by interfluve depth. These were obtained (Mitchell, 2005) by segmenting the data in Fig. 2c between points of local minimum and maximum depth and aligning the hillcrests of those segments. The characteristic profiles in Fig. 2d were then obtained by averaging those segmented profiles and mirroring the data about the origin. Shallower than 400 m, terrain between canyon heads is rounded and the characteristic interfluve morphology can be approximated by parabolas (dotted curves in Fig. 2d; values to right are RMS misfits). Two seismic lines of R/Vs *Robert Conrad* (Lamont–Doherty Earth Observatory, unpubl. data) and *Gulf Seal* (Schlee et al., 1976) show that the uppermost slope has prograded. The smooth topography identified here, therefore, overlies the older slope so any pre-existing relief of slope channels has been smoothed out by the later deposits, a diffusive-like behaviour.

Deeper than 400 m, canyon walls are almost exactly linear on average and interfluves are sharp (curvature around the graph origin is a resolution artefact). In subaerial geomorphology, such linear slopes are termed “threshold hill-slopes” (Carson and Petley, 1970), where frequent superficial landslides lead to the terrain adopting gradients representing the stability limit of regolith during high rainfall conditions. By analogy, these canyon walls are probably also shaped by surficial landslides, as indicated by sparker seismic images collected here (Malahoff et al., 1982), generating the canyon wall gullies seen in Fig. 2a.

To provide an alternative way of characterising the transition from rounded to sharp terrain, we calculated the curvature and local maximum gradient of the Atlantic data. Curvature was represented by ∇^2H calculated from the multibeam data by finite differences (Wessel and Smith, 1991). Median and inter-quartile range of curvature and gradient are plotted versus depth in Fig. 6a. Progressive steepening with increasing depth is associated with the onset of incision, i.e., with canyon heads. The inter-quartile range of curvature increases from 300 to 500 m in Fig. 6, reflecting the developing canyon relief. This transition coincides with surface grain size decreasing progressively from gravely sand, muddy sand, sandy mud to clayey silt, with the latter transition (the “mud-line”) at 350 m depth along the southerly part of the area (Fig. 2b, inset). Published maps show this grading pattern continuing along-strike (Southard and Stanley, 1976; Stanley and Wear, 1978; Keller et al., 1979; Stanley et al., 1983), with the mud-line at around 300 m (Stanley and Wear, 1978). Drilling 7 km west of Fig. 2 recovered predominantly sands to 310 m below seafloor (AMCOR 6007, Hathaway et al., 1976, 1979). In the depth range of smooth topography, therefore, the bed is dominantly sandy. Coinciding with it, median curvature is negative, so more terrain is convex-upwards than is concave-upwards. This is a feature of diffusive landscapes where convex hillslopes occupy more terrain area than channels, which are more localised areas of upwards concavity.

2.2. Monterey Bay multibeam sonar data

Fig. 3 shows abundant smooth topography and upwards-convex regions between channels (Greene et al., 2002). Faults (represented by grey lines on Fig. 3b) crossing canyon heads in the northwest (around 36° 55’ N, 122° 20’ W) are seismically inactive (McHugh et al., 1997), but seismic data show them offsetting Miocene strata (Nagel et al., 1986). Sedimentary processes have

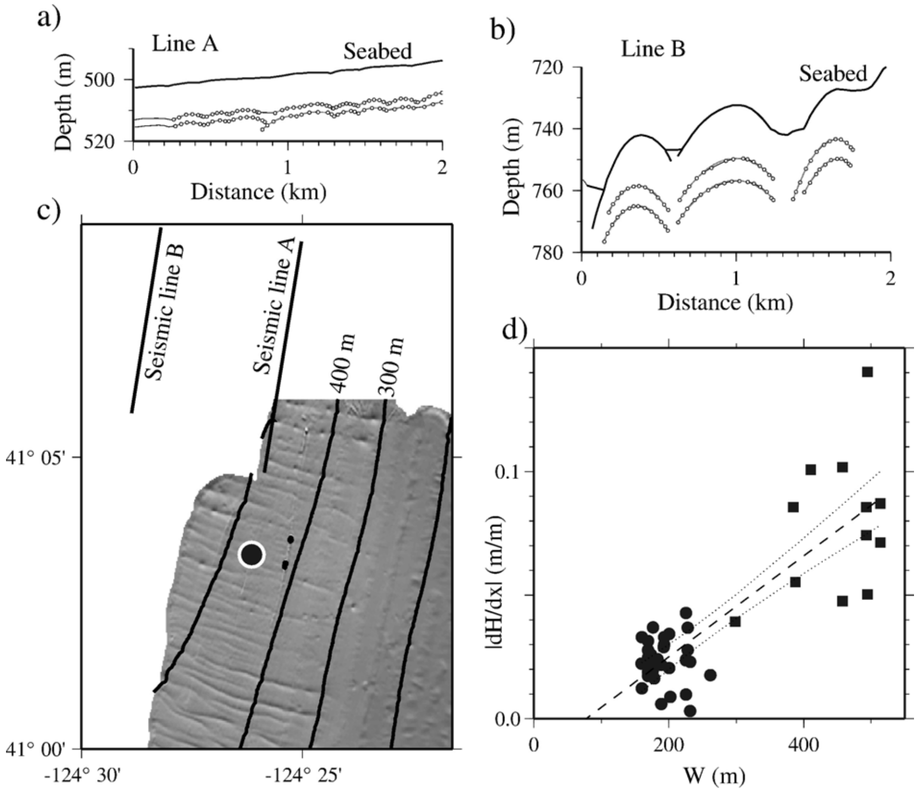

Fig. 5. (a) and (b) Interpretations of interfluve topography from two lines of Huntec boomer seismic data (Field et al., 1999) acquired parallel to the regional slope in (c). The bold curves show parabolas fitted through sections of the data. Small solid circles show points were the original seismic horizons were digitised. (c) Shaded relief image of bathymetry from northern California showing gullies in high-resolution Simrad EM1000 multibeam sonar data of the continental slope (Goff et al., 1999). Solid circle locates a current meter deployment (Cacchione et al., 2002). (d) The along-slope gradient $|\partial H/\partial x|$ of the fitted parabolas in (a) and (b) are shown plotted against the spacing of the channels W (average of the distances to the two adjacent channels). The dashed line shows a least-squares regression with uncertainty in predicted mean $|\partial H/\partial x|$ given by the dotted lines.

left the modern seabed smooth with no evidence of the older faults. Sediments in this area may include sand spilled over the outer shelf (Edwards, 2002), but Quaternary sediments away from active channels are otherwise muddy (Greene, 1977; Nagel et al., 1986; McHugh et al., 1997; Paull et al., 2005a).

Although Smooth Ridge has a subdued surface (Fig. 3b) (Greene et al., 2002), seismic data reveal shifting channels, slumps and sediment waves (Jordahl et al., 2004), a relief that has attenuated towards present. Sediments around fluid expulsion sites here are hemipelagic (Barry et al., 1996) and low-backscattering in deep-tow sidescan data (Orange et al., 1999) suggests widespread mud. Measured accumulation rates are low, with a lack of Holocene deposits implying non-deposition or erosion at present (Jordahl et al., 2004).

To facilitate comparison with the Atlantic data, Fig. 6b and c show gradient and curvature statistics for the two areas outlined in white in Fig. 3a calculated after filtering the bathymetry data to the same spatial resolution as the Atlantic data. In Monterey Bay, the shelf edge is abrupt, so median gradient steepens sharply at ~150 m. Within the NW area, median curvature is negative at 300 m as in the Atlantic, reflecting a generally upward-convex terrain. Within the E area, median curvature is instead nearly zero at 300 m, reflecting the greater density of channels.

Fig. 7 (left) shows profiles of individual hillslopes derived by segmenting the cross-sections between points of local maxima and minima (from ridges marked with dots in Fig. 3a, inset). Slopes wider than 2 km were excluded (explained in Section 3.3). Apart from one horizontal hillcrest with rounded edges in one 200–300 m profile, the remaining upper-slope profiles are more characteristically smooth parabolic interfluves, in particular in the 300–400 m depth range, whose average is well-approximated by a parabola (Fig. 7, right). Below 400 m, profiles are angular because of landsliding, but there is a greater diversity of shapes, with some interfluves also smoothly parabolic.

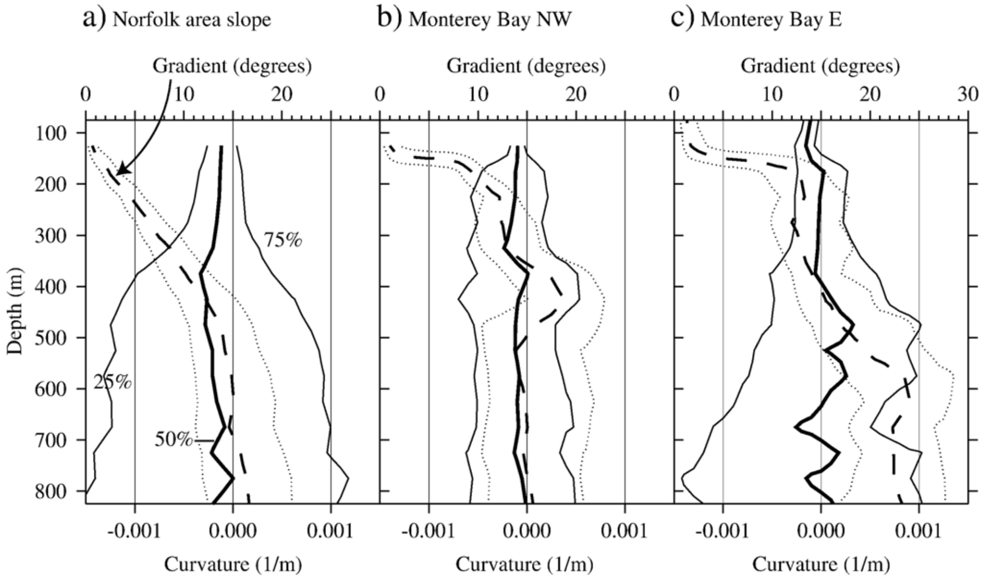

Fig. 6. Variation of curvature and gradient characteristics versus depth for (a) Fig. 2 (black outlined area) and (b, c) Fig. 3a (two white outlined polygons). Curvature represents $\nabla^2 H$ and gradient is the maximum local gradient at each grid point, both calculated using finite differences (Wessel and Smith, 1991). These values were sorted according to depth and the curves show the median average value (bold and bold dashed lines) and the inter-quartile range of values (fine and dotted lines, for curvature and gradient, respectively).

2.3. New Jersey slope seismic reflection data

Fig. 4 shows interpreted stratigraphy of high-resolution seismic data collected with a deep-towed hydrophone towed along the slope (Robb et al., 1981b). It shows aggraded ridges of Pleistocene muds and silts (Hathaway et al., 1976), developing smooth parabolic-like interfluves, while non-deposition or intermittent erosion occurred along channels. Later sediment on the left ridge drapes the previous topography, while the right ridge steepened until slumping (grey lines mark sediment discontinuities). Growth of ridges by progressive aggradation (rather than entrenchment along channels) is also common in other seismic and sediment profiler data of continental slopes (McGregor and Bennett, 1977; McGregor et al., 1979; Robb et al., 1981a; Alonso et al., 1985; Farre, 1987; Pratson et al., 1994; Casas et al., 2003).

2.4. Eel River slope seismic reflection data

Fig. 5c shows an image of the bathymetry of the upper slope north of the Eel River (Goff et al., 1999), revealing numerous shallow gullies. Fig. 5a and b show interpretations of two lines of boomer seismic images (Field et al., 1999) collected along-slope in different water depths located in Fig. 5c. They reveal that the gullies increase in relief and increase in spacing (i.e., converge) down-slope. Flows causing channel erosion probably originated from muddy suspensions generated by wave action in shallow water which spilled over the shelf (Wright et al., 2001; Scully et al., 2002). From a larger dataset, intefluves had greatest relief during times of sea-level low-stands, when re-suspension of shelf

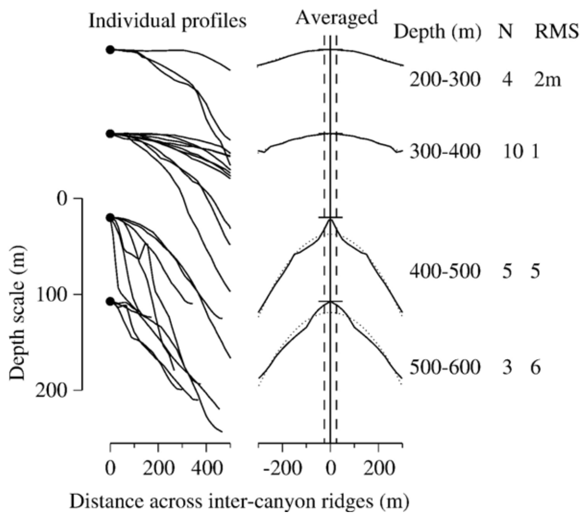

Fig. 7. Hillslope relief profiles (left graphs) derived by segmenting the data in the cross-sections of Fig. 3a between points of local maximum and minimum depth and then aligning at common depth values (procedure as in Mitchell (2005)), using hillcrests marked by dots in Fig. 3a, inset). Right graphs show the data averaged as in Fig. 2d.

sediment was probably more frequent and vigorous (Spinelli and Field, 2001). The interfluves are almost exactly parabolic and their coherence with reflectors below them suggests that their topography was stable when they were exposed on the sea floor (i.e., a steady-state morphology).

According to Alexander and Simoneau (1999), surface sediments here are mostly silt. At the location of the two seismic lines, average grain size decreases systematically with depth from $\phi=8$ at 500 m to $\phi=8.5$ at 750 m ($\phi=-\log_2$ (grain size in mm)), from down-slope sedimentary processes preferentially transporting fine grade material. Accumulation rates (^{210}Pb) increase from 0.2 g/cm^2/yr at 300 m to 0.3 g/cm^2/yr at 700 m. X-radiographs and physical properties reveal strong bioturbation (Sawyer et al., 1997).

3. Interpretation using the diffusion transport equation

3.1. Diffusion equation derivation

In marine settings, the seabed can aggrade by particles accumulating from the overlying water column, so a sediment supply parameter D is often added to the diffusion transport equation:

$$\frac{\partial H}{\partial t} = K\nabla^2 H + D \tag{1}$$

where H is the bed topography and K is a mobility parameter (m^2/s) (Webb and Jordan, 1993). The Laplacian $\nabla^2 H$ represents the terrain's curvature. Eq. (1) implies that sediment accumulates in depressions (areas of positive $\nabla^2 H$, hence positive $\partial H/\partial t$) and erodes from hills (areas of negative $\nabla^2 H$) if $|K\nabla^2 H| > D$. In the absence of other effects sharpening relief, these tendencies cause topography to become smooth over time, a property noted in the various datasets above.

To understand whether and how different submarine processes are likely to lead to diffusive tendencies, it is worth revisiting the logic behind the model. It originates in hillslope studies (Culling, 1960, 1963; Kirkby, 1971) by combining an argument for how soils creep down-slope with an assumption that mass is locally conserved. In linear creep (McKean et al., 1993;

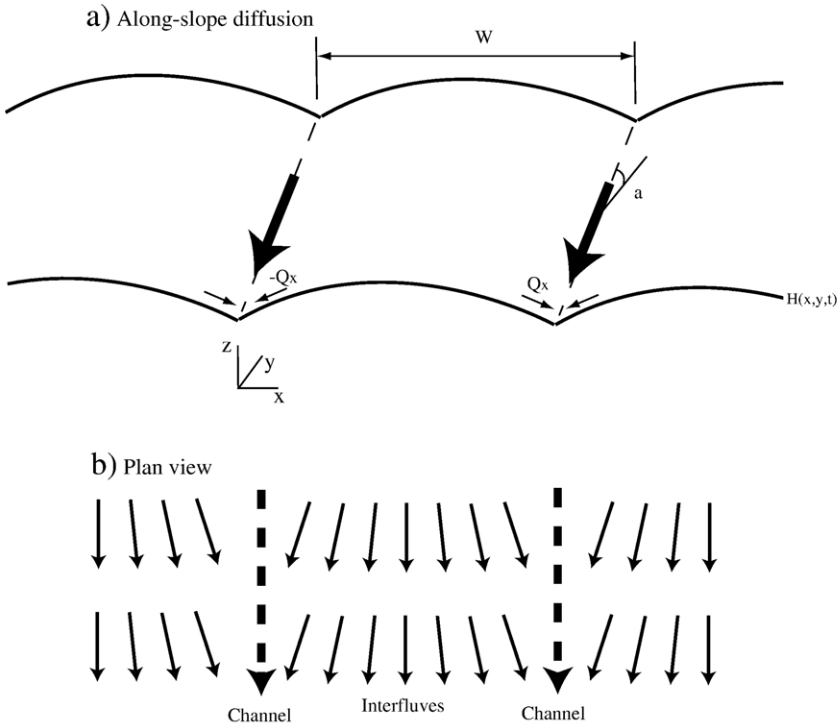

Fig. 8. (a) The regional slope is incised by small sedimentary mass flows (turbidity currents) travelling down the channel thalwegs (large arrows). In a diffusion model interpretation, the areas between thalwegs respond to sediment removal according to a diffusion equation and the parabolic form is produced by the along-slope component of transport (time-averaged flux Q_x and small arrows). (b) The pattern of model sediment transport in plan view, with intermittent flow erosion down channels (dashed lines) and more widespread movements on interfluves (vector orientations exaggerated for effect).

Small et al., 1999), soil moves at rates proportional to the local surface gradient:

$$Q = -K\rho_s \frac{\partial H}{\partial y} \tag{2}$$

where Q (kg/m/s) here is the solid mass flux in the down-slope direction (y (m)) per unit width of slope and ρ_s (kg/m^3) is the soil dry density. The continuity relation (conservation of mass) represents how a spatial change in soil flux causes erosion or deposition:

$$\frac{\partial H}{\partial t} = -\frac{1}{\rho_s}\frac{\partial Q}{\partial y} \tag{3}$$

Differentiating Eq. (2) in y and substituting in Eq. (3) then leads to a diffusion equation in H:

$$\frac{\partial H}{\partial t} = K\frac{\partial^2 H}{\partial y^2} \tag{4}$$

Eq. (1) can be obtained by generalising to two dimensions.

3.2. The smooth, parabolic interfluve form as a steady-state solution

In lowland diffusive landscapes, erosion along streams provides a boundary condition to the intervening hillslopes. If the flux of removed material is constant, the solution to Eq. (4) is a simple upwards-convex parabola (Kirkby, 1971; Allen, 1997), a shape typical of lowland hills. More generally, hills are expected to acquire rounded forms simply because, in a steady-state geometry, soils must creep faster towards channels to accommodate removal of increasing amounts of upslope soil mass, which implies steepening (Gilbert, 1909).

In a diffusion model interpretation (Fig. 8a), the geometrically analogous rounded interfluves form in periods between channelized flows, or during widespread dilute sedimentary flows occurring at the same time as channelized flows, involving a small component of sediment movement along the regional slope. Accordingly, the planform of transport is in the local direction of maximum gradient (Fig. 8b) and the parabola arises from the small along-slope component of this transport. If Q_x represents the time-averaged flux of material eroded from one side of each channel's margins during sedimentary flows (Fig. 8a) and W is the channel spacing, the model topography responds to boundary conditions of $Q=-Q_x$ at $x=0$ and $Q=Q_x$ at $x=W$. The steady-state solution to Eq. (1) for areas between channels is then:

$$H = \frac{Q_x}{K}x - \frac{Q_x}{WK}x^2 \tag{5}$$

H is positive upwards, measured from an origin at one of the channels (Fig. 8a) and chosen here to migrate vertically with the accumulating sediment surface (ignoring D in Eq. (1) as it does not affect interfluve shapes). Gradient in the down-slope direction is uniform so that transport fluxes in y can be ignored because they produce uniform translation.

In subaerial landscapes, threshold hillslopes modified by some diffusion leave hillcrests rounded rather than perfectly sharp, depending on the relative importance of diffusion and landsliding (Anderson, 1994; Roering et al., 1999). Some rounded ridges are geometrically analogous (e.g., profile 4 from top at 27 km in Fig. 2c), i.e., intermediate between parabolic and sharp.

3.3. Development with time (New Jersey slope)

The style of accumulation depicted in Fig. 4 is similar to that of temperature in the analogous problem of a heating plate with constant temperature boundaries (Carslaw and Jaeger, 1959), here with erosion or non-deposition along channels acting as the boundary conditions. To illustrate it, the lower-right curves in Fig. 4 show a finite difference calculation in which an array of 200 equally spaced nodes representing an along-slope profile of seabed topography was repeatedly adjusted by adding an elevation element to represent uniform hemipelagic fallout. At each time step, a transport flux was computed from the along-slope bed gradients (Eq. (2), using elevation differences for $\partial H/\partial y$) and bed elevation change calculated from Eq. (3). Boundary conditions of fixed elevation were imposed at the dashed lines. Numerical stability was maintained by using small $\rho_\sigma K$ and many iterations (4×10^5). Model values are omitted because time- and length-scales are arbitrary, rather the purpose is to illustrate evolutionary style.

The topography evolves towards a steady state in which material supplied by fallout is balanced by erosion along channels, at which stage the surface is parabolic. Although generally similar to the data, some differences of detail are apparent. For example, in the model, influence of the boundaries progressively migrates inwards, but the data show only weak evidence for this, such as pinchouts of strata; actual deposition is more unsteady and irregular. Note that migration of boundaries results in interfluves with flat central regions and rounded edges, features similar to those of some Monterey Bay hillcrests (Fig. 3a, inset). Hence, flat interfluves could represent transient stages, which are expected to be more common in larger features.

3.4. Down-slope trends (Eel River slope)

Q_x likely increases down-slope for several reasons and, provided that erosion does not excessively steepen slopes to cause landslides, this potentially allows us to investigate how interfluve geometry responds to varying Q_x. First, if flows initiated above the area were active in only one channel at a time, the frequency and net erosive effect of many flows increases down-slope simply because the channels converge so that flows in multiple channels in the upper slope contribute to single channels lower in the slope (Mitchell, 2004). Second, if several tributaries were simultaneously active (e.g., flows triggered by a storm), suspended sediment discharge in the flows increases down-slope, analogous to river discharge increasing with increasing contributions from tributaries. In some studies of stream bed erosion, erosion rate was found to be proportional to bed shear stress (Howard and Kerby, 1983). If shear stress controls erosion by turbidity currents, erosion rate should be correlated with sediment discharge, although whether the relationship is exactly linear or not depends on other factors (Mitchell, 2006). Third, the erosive power of individual flows may increase as they incorporate eroded material (Parker et al., 1986).

The third effect is difficult to predict but the first two effects should lead to Q_x increasing roughly in proportion to channel spacing W (if 'n' channels converge to n/a channels, flow frequency should increase on average by a factor 'a' which is proportional to average W). The model Q_x/K is proportional to along-slope gradient $|\partial H/\partial x|$ so in Fig. 5d $|\partial H/\partial x|$ is plotted versus W (W is the average of the distances to the two adjacent channels either side of the channel being measured). The graph scatter reflects the variability of interfluve forms but average $|\partial H/\partial x|$ roughly doubles as W increases from 200 to 400 m, close to the doubling expected from Q_x/K proportional to W. Thus, some systematic variations in interfluve morphology are also as expected from diffusion.

4. Discussion

In summary, characteristics typical of diffusive hillslopes with erosion along channels providing boundary conditions include: small interfluves commonly have smooth parabolic shapes, their growth patterns revealed in seismic reflection data can be similar to transient solutions, and down-slope trends in interfluve along-slope steepness can be as expected from varied channel erosion. Given this geometrical compatibility, then, does the parabolic interfluve morphology result from true diffusion or is it merely fortuitous? Except in carbonate and other chemically mobile systems, the assumption of conservation of mass (Eq. (3)) is usually adhered to, so to evaluate whether true diffusion occurs we are mostly interested in whether sediment flux is down-slope and has a magnitude proportional to bed gradient (Eq. (2)). If true diffusion does occur, the model implies that sediment transport is strongly controlled by local bed gradient, i.e., by gravity, and the shapes of interfluves and their evolution in turn may provide information on sediment transport, as they do in subaerial hillslope studies. On the other hand, suspended sediment transported by currents does not necessarily follow Eq. (2) so the answer to this question is not generally straightforward.

Accurate evaluation will require arrays of long-term current meter and other data to derive transport rates across interfluves to be compared with the patterns of Holocene accumulation. If slope morphology reflects conditions during earlier periods when sea-level was lower, e.g., during the LGM, methods will be needed to predict currents during these times. In the absence of such information, the following initiates discussion by commenting on likely influences based on other studies in the literature.

4.1. Influence of oscillating currents

4.1.1. Gravity effect on saltating particles

The effect of gravity on saltating grains leads to a down-slope component of bedload flux proportional to bed gradient and thus an element of true diffusion, potentially explaining the smooth morphology of the sandy central Atlantic uppermost slope (Fig. 2). Currents there are often sufficiently strong to mobilise sand (Csanady et al., 1988) and would have been stronger during the LGM, when storm waves would have been more strongly felt because of lowered sea-level. Tidal currents would have also been stronger because deep-water tidal range was larger (Egbert et al., 2004). Tidal currents in the outer shelf are approximated by the ratio of water volume moved to accommodate tides across the shelf to shelf-edge water depth (Fleming, 1938), a ratio that was also larger with lowered sea-level.

The following equation has been used to represent bedload transport flux of sand:

$$\mathbf{Q} = G|\mathbf{u}|^m(\mathbf{u} + \lambda|\mathbf{u}|\nabla H)/g \tag{6}$$

where $\mathbf{u}$ is the current vector (m/s), G is a constant coefficient, g is acceleration due to gravity (m^2/s) and λ is 1/tanα, where α is the angle of repose of the sediment (bold symbols represent vectors and |…| the vector magnitude). The exponent 'm' is typically chosen to be 2. Eq. (6) was derived for fully developed bedload by extending an energetics argument (Bagnold, 1963) to two-dimensional slopes (Bailard and Inman, 1981; Huthnance, 1982a,b).

Eq. (6) suggests that, if currents reverse such that the vector average $<\mathbf{u}>$ is small compared with $\lambda<|\mathbf{u}|>\nabla H$, the second term dominates ($<\ldots>$ denotes the mean taken over the cycle). Agitation of bedload can therefore move sand parallel to ∇H at rates proportional to $|\nabla H|$, satisfying Eq. (2). A diffusive-like evolution of bed topography would be expected with $K\sim<|\mathbf{u}|>^3$. Furthermore, even if $<\mathbf{u}>$ is significant compared with $\lambda<|\mathbf{u}|>\nabla H$, a diffusive-like evolution is still expected from the down-slope component because residual current $<\mathbf{u}>$ is commonly parallel to contours so that it leads to contour-parallel translation of sand with less influence on morphology.

4.1.2. Mud accumulation and erosion

Where the interfluves have aggraded, average accumulation rates increase away from channels. Currents due to internal tides are well known to be enhanced in canyons (Keller and Shepard, 1978; Shepard, 1979) and numerical modelling by Cacchione et al. (2002) using multibeam bathymetry suggested enhanced shear stress due to breaking internal waves along central Atlantic canyons with winter stratification. Cacchione et al.'s model for the Eel slope implies slightly larger bed stresses along gullies than over adjacent interfluves, with a gradual change in between.

Predicting patterns of long-term accumulation rates is complicated because, although instantaneous deposition rates are predictable from particle settling through the viscous sub-layer (McCave and Swift, 1976), bottom currents on the slope vary in strength, alternately causing deposition and erosion, while erosion resistance is variably affected by stress-hardening, stabilising biological particles and mucus, compaction, etc (Krone, 1976; McCave, 1984; Parchure and Mehta, 1985; Mehta et al., 1989; Perkins et al., 2004). Nevertheless, accumulation rates are generally expected to be smaller where bed stresses are generally larger. Thus, transport flux may not obviously be related to bed gradient and instead the smooth parabolic shapes of muddy interfluves could arise fortuitously.

4.2. Transport by gravity currents

Gravity flows originate from wave-agitated suspensions (Wright et al., 2002), slope failure or cascades of shelf water made dense by cooling, evaporation or freezing (Shapiro et al., 2003; Ivanov et al., 2004). Bedload transport by gravity currents potentially causes diffusion because bedload flux increases as the currents speed up onto steeper gradients, leading to erosion across the intervening convex-upwards regions similar to Eq. (4). This can be shown (Mitchell, 2006) by combining the effect of gradient on the current speed (Komar, 1977) with the bedload flux dependence on current speed (Bagnold, 1963). Diffusion, however, would apply only to the flow-wise direction and does not obviously explain the smoothly parabolic interfluve morphology sub-perpendicular flow direction. Furthermore, advective-type evolutions of flow-wise topography are instead expected from deposition of mud suspended by waves (Friedrichs and Wright, 2004), bed erosion by flow intensified on steep gradients (Mitchell, 2006) or by incorporating bed sediment (Parker et al., 1986).

Izumi (2004) envisions slope gullies initiating by widespread sedimentary flows becoming unstable and gathering to form channels. Interfluves then grow from sediment depositing in low stress regions between gathering flow. As the relief of spurs between channels grow, they cause flow divergence as illustrated in Fig. 8b. Its effect can be shown simply if the flow is assumed to be in equilibrium but sufficiently fast so that Coriolis effects are secondary. The divergence effect on the specific sediment flux Q_{sy} can be obtained from the continuity relation ($\partial Q_{sy}/\partial x=-\partial Q_{sx}/\partial y+D$) with $Q_{sx}=Q_{sy}\tan\alpha$, where Q_{sy} and Q_{sx} are the down- and along-slope flux components, α is the down-gradient direction relative to the regional slope and D is the accumulation rate introduced earlier. Thus, the down-slope change in solid flux in the current is:

$$\frac{\partial Q_{sy}}{\partial x}=-Q_{sy}\frac{\partial(\tan a)}{\partial y}+D \tag{7}$$

where $\partial\tan\alpha/\partial y$ is the bathymetry contour curvature.

During equilibrium flow, bed shear stress $\tau_0\infty(Q_sS)^{1/2}$ where S is flow-wise gradient (Komar, 1977). Thus, if D in Eq. (7) is comparatively small and erosion or deposition rate is related to bed shear stress (e.g., McCave and Swift, 1976; Howard and Kerby, 1983; McCave, 1984), divergence will lead to a rate of bed change that is related to bed curvature analogous to that in Eq. (4) but with opposite sign. Despite the opposite sign, parabolic interfluves are regions of constant curvature so a divergence effect should lead to uniform erosion or deposition rate and hence this form can become stable. The divergence effect here is similar to that suggested to cause levee growth (Imran et al., 1998) and interfluve structures such as Fig. 4 have been suggested to accumulate from the finer particles of turbidity currents (Robb et al., 1981b).

4.3. Bioturbation

Fish, crabs and other organisms are significant geomorphologic agents in stirring and eroding continental slopes (Dillon and Zimmerman, 1970; Stanley, 1971; Warme et al., 1978; Valentine et al., 1980; Malahoff et al., 1982; Forde et al., 1984; Paull et al., 2005b). Although organisms create relief at small scales (e.g., mounds of sediment expelled from burrows), they may contribute to topographic diffusion at larger scales (Kenyon and Turcotte, 1985). Sediment suspended by bottom feeders falls back to the bed under gravity, a process that may move sediment down-gradient similar to the gravity effect on saltating sand. Burrow collapse also causes small down-slope movements. Although the geometric details are poorly known, burrowing could have effects in translating sediment to and from the surface (Wheatcroft et al., 1990) analogous to those of animal burrowings in soils which cause forms of hill-slope diffusion (Gabet, 2000).

Vertical mixing rates D_b from bioturbation are estimated by modelling radiometric profiles in sediments. Volumetric rates based on ^{210}Pb are ~1 m^2/ky near shelf-break depths (Soetaert et al., 1996; Middelburg et al., 1997; Henderson et al., 1999), reaching 20 m^2/ky using the shorter half-life isotope ^{234}Th in a nutrient-rich area off North Carolina (Green et al., 2002). Although D_b can vary with nutrients, etc (Anderson et al., 1994; Smith et al., 2000; Green et al., 2002), it commonly decreases sharply with increasing water depth below the shelf edge (Anderson et al., 1988; Soetaert et al., 1996; Middelburg et al., 1997; Henderson et al., 1999; Schmidt et al., 2002).

Inferring horizontal movements implied by these data is problematic because they depend on burrow geometry and other factors. Activities of bottom feeders, which often dominate bioturbation, lead to much larger horizontal than vertical displacements (in one study, horizontal D_b was an order of magnitude larger than vertical D_b (Wheatcroft, 1991)). Hence, although the above D_b values are small, they do not rule out significant horizontal displacements.

As different species cause different geometries of sediment movement and their occurrences vary with depth and environmental conditions (e.g., Day et al., 1971), it is not strictly possible to infer that K will vary in the same way as D_b. Nevertheless, the observed biological activity in the upper slope and sharply declining D_b with water depth suggest that the frequency of benthic resuspension events probably declines sharply down the slope, which may help to explain why the bathymetry in Fig. 2a is smooth around 200–300 m but sharp below 400 m.

4.4. Other processes smoothing topography of mud

If deposition or erosion is enhanced in certain areas, suspended sediment concentration in the bottom nepheloid layer changes and opposes further deposition or erosion (i.e., if all sediment falls from suspension, no further deposition can occur). Eddy diffusion within the bottom nepheloid layer (Appendix A1) or water translation, however, redistributes local changes in concentration, allowing the process to continue and facilitating morphological change. The following then smooth mud topography, if no other processes create relief.

4.4.1. Quiescent flow

Where the bottom nepheloid layer is slow, flow expands and slows over depressions, leading to smaller bed shear stress and deposition. In modelling growth of mudwaves, Flood (1988) adapted analytical expressions for airflow over sinusoidal topography (Queney, 1948). When flow is moderate, streamlines are out of phase with topography, leading to climbing mudwaves, but if slower they are in phase, promoting deposition in depressions. According to Flood, the latter stage occurs when the spatial wavenumber of topography $k=2\pi/L<k_f$, where $k_f=f/u$, L is topography wavelength and f is the Coriolis parameter ($f=2\Omega\sin\phi$ where Ω is Earth's rotation rate (7.27×10^{-5} rad/s) and ϕ is latitude). Thus, for $\phi=36°$ and for current speeds of 5 and 20 cm/s typical of the Atlantic upper slope (Csanady et al., 1988), flow should be quiescent for topography of wavelength >4.3 km and >17 km, respectively. As flow is often slower than 5 cm/s, it should be quiescent at kilometre scale for much of the time. Weatherly (1993) tested this idea by observing flow over 5.5 km wavelength mudwaves at 40° S in the Argentine Basin. Flood's analysis predicted flow to be quiescent when less than 9 cm/s and the transition in flow behaviour was indeed observed at a similar flow speed of 12 cm/s.

Bottom observations along the Atlantic (Doyle et al., 1979; Csanady et al., 1988; Churchill et al., 1994) and Pacific (Cacchione et al., 2002) slopes show silt grade sediment repeatedly resuspended by currents when flow is not so quiescent. Furthermore, flow should not be quiescent for less than the wavelengths given above according to Flood's arguments. Slope accumulation might therefore be expected to be asymmetric with respect to topography or at least not necessarily enhanced in depressions. This inconsistency with data is potentially reconcilable if sediments deposited during the turning phase of the currents, when flow is quiescent, become rapidly stabilised against subsequent erosion. Net accumulation could then be biased towards quiescent conditions. Stabilisation by polymeric mucus (Perkins et al., 2004) might provide such a mechanism, as mucus can be excreted quickly compared with the time over which internal wave currents reverse.

4.4.2. Declining influence of surface-originating disturbances with depth

Where oscillating currents decline with depth, shear stress on the top of a hill can be greater than in adjacent valleys, causing erosion or slow deposition on hillcrests relative to valleys. The current data of Csanady et al. (1988) for example show high frequency (period <11 h), diurnal and wind-driven oscillations declining sharply to 1000 m depth. From deep water approximations (Masselink and Hughes, 2003), speeds associated with storm waves of 20 s period decline by 39% from 200 to 250 m and shear stress by 84%. Other factors leading to enhanced speeds towards shallow depths include tidal energy becoming concentrated into shallower water and wind momentum input having less water mass to accelerate.

Although tidal oscillations are often enhanced in canyons (Shepard, 1979), topographic interactions can lead to them becoming attenuated. For example, data from a current meter deployed at 1220 m within a 300-m-deep canyon off Nova Scotian (Csanady et al., 1988) showed the relief blocking strong currents of topographic waves (currents due to Gulf Stream rings), leaving mean speeds within the canyon 40% smaller than on the adjacent open slope. A similar effect was observed 50 km northeast of Washington Canyon (McGregor, 1979).

Below the upper slope, bed shear stress is caused by tidal, internal and topographic waves, which vary slowly with water depth. As currents on the open slope are close to threshold of deposition (Csanady et al., 1988) and deposited sediment often becomes resistant to erosion (McCave, 1984), however, even minor variations in shear stress could potentially affect morphology significantly.

4.5. Viscous creep

Clay rich sediments can creep slowly under differential stress markedly below their peak strengths (Silva and Booth, 1984). Creep has been suggested to have affected central Atlantic slope sediments (Bennett et al., 1977; McGregor and Bennett, 1977; McGregor et al., 1979; Nelsen and Bennett, 1981; Bennett and Nelsen, 1983; Silva and Booth, 1984) and may explain widespread evidence for slope failure (Knebel and Carson, 1979) despite near-surface geotechnical properties implying that the sediments are stable (Booth, 1979; Keller et al., 1979; Almagor et al., 1982).

Evidence of mass-movements (though not necessarily creep) include slump scarps and missing surface sediments in sparker seismic profiles, immediately east of the area of Fig. 2, and from the slope 50 km northeast of Washington Canyon (Malahoff et al., 1980; Malahoff et al., 1982). ALVIN dive 807 traversed steep but otherwise featureless walls of two canyons and an intervening ridge in Fig. 2a, so movements were not recent (Malahoff et al., 1982). Sand balls within silty clays and contorted bedding in cores recovered from around Baltimore and Wilmington canyons were interpreted as evidence of creep (Bennett et al., 1977; McGregor and Bennett, 1977; McGregor et al., 1979). Cobbles and boulders observed during ALVIN dive 765 near Baltimore Canyon, including a 2–3 m slab of beachrock at 456 m depth on a gradient of only 2.5°, were interpreted to have been emplaced by sliding or creep (Malahoff et al., 1982). Seismic and bathymetry data shown by Malahoff et al. reveal that the exotic clasts occur on a spur between canyon heads where the slope is generally smooth and rounded, whereas McGregor et al.'s cores were recovered from within canyon heads where mass-wasting may have occurred.

Rheology of clay-rich soils is frequently Bingham-like (van Asch et al., 1989; van Asch and van Genuchten, 1990) so that shear stress:

$$\tau = \tau_c + \mu \left| \frac{\partial v}{\partial z} \right|; \qquad \tau > \tau_c \tag{8}$$

where μ is the Bingham viscosity, $\partial v/\partial z$ is the velocity gradient (z is depth below the sediment surface, v is down-gradient velocity parallel to the soil surface) and τ_c is a critical shear stress. Tests on clay-rich Atlantic USA slope sediments (Booth, 1979; Silva and Booth, 1984) found an initial short primary phase of rapid creep, followed by a secondary phase of slower creep in which strain rate was constant for a given applied stress, as expected from Eq. (8). The primary phase was less significant at small deviatoric stress, so the secondary phase should be more important for slope sediments experiencing only weak loading.

Although only a crude approximation of rheological behaviour (Ter Stepanian, 1975), Eq. (8) is useful for suggesting how strain rate may depend on loading. In surficial sediment, loading stress τ originates primarily from sediment weight ($\gamma' z \sin\alpha$, where γ' is the submerged bulk density of the sediment (allowing for buoyancy) and

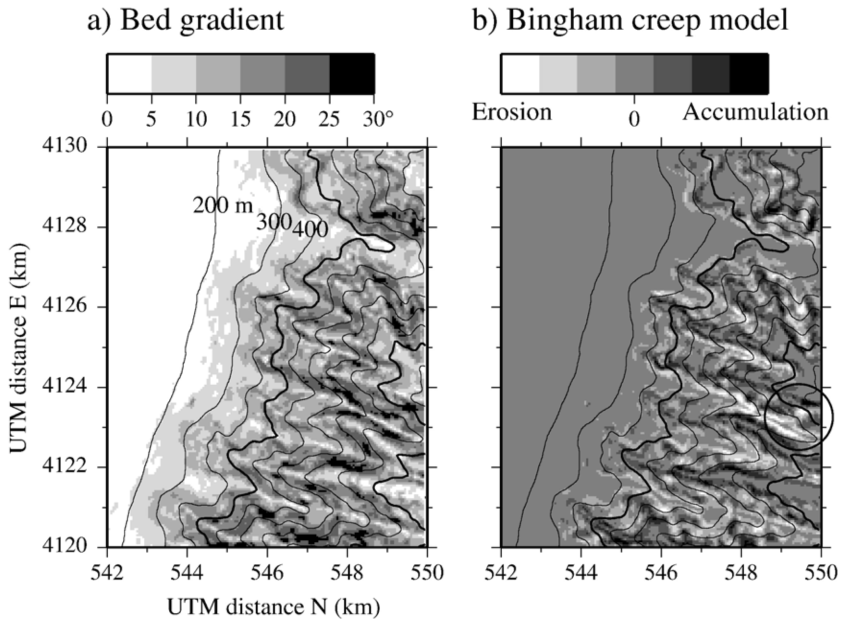

Fig. 9. (a) Maximum local bed gradient. (b) Pattern of erosion/accumulation rate predicted by a model in which a uniform near-surface sediment layer with a Bingham viscous-plastic rheology, with a threshold stress corresponding to a bed gradient of 10°. Circle highlights an area of erosion of spurs and deposition within canyon wall gullies that clearly cannot be sustained (as this topography is preserved), therefore implying that creep does not occur persistently in this manner or is too slow to affect morphology. The bathymetry data from Fig. 2 were first projected into a Universal Transverse Mercator grid (50 m node separation) and smoothed with a 5×5 averaging filter before applying the flux calculations. Area is centred on approximately 37° 15' N, 74° 30' W (north of centre of Fig. 2a).

α is the bed gradient angle). Rearranging Eq. (8), the deformation rate is:

$$\mu\left|\frac{\partial v}{\partial z}\right| = \gamma' z\sin\alpha - \tau_c; \qquad \gamma' z\sin\alpha > \tau_c \tag{9}$$

Silva and Booth (1984) and Booth (1979) concluded that creep is geologically significant for gradients greater than 10° for the Atlantic slope sediments they studied. Predicted deformation in a 50 m layer was insignificant below 10° but reached 0.5 m/yr at 10°, implying significant movements over ky-timescales from self-loading. Seismic images of terracettes produced by creep elsewhere (Almagor and Wiseman, 1982; Hill et al., 1982; Silva and Booth, 1984) imply movement over weak deforming layers, similar to "depth creep" in subaerial slopes (Selby, 1993).

If a uniformly deforming sub-surface layer of small vertical thickness W_c passively carries a thickness W_o of sediment above it, the volumetric down-slope flux would be:

$$|Q_c| = \left|\frac{\partial v}{\partial z}\right| W_c\left(W_o + \frac{W_c}{2}\right) \tag{10}$$

Using $|\partial v/\partial z|$ from Eq. (9), Q_c can be written in terms of gradient above a threshold:

$$\mathbf{Q}_c = -K_c(|\nabla H| - S_0)\frac{\nabla H}{|\nabla H|} \tag{11}$$

where S_0 is threshold gradient corresponding to τ_c, $|\nabla H| \approx \sin\alpha$, $\nabla H/|\nabla H|$ is a unit vector in the direction of ∇H to provide direction for $\mathbf{Q}_c$ and $K_c = W_c(W_o + W_c/2)\gamma' z/\mu$.

Potential morphological consequences were explored by assuming that a layer of weakly consolidated sediment of uniform thickness and properties was deposited at some time in the past over the entire upper slope. Eq. (11) was then applied to the slope bathymetry by calculating Q_c with $K_c = 1$ and $S_0 = \tan 10°$. Changes in bed topography were then calculated from the continuity relation $\partial H/\partial t = -\nabla \cdot Q_c$.

The results (Fig. 9b) show erosion along the margins of ridge crests but small changes immediately at the crests, a tendency that would sharpen crests and thus might help to explain the observed angularity of ridges (Fig. 2d). The predicted accumulation in lower canyon walls (black in Fig. 9b) evidently does not occur in practice, but this material could be removed by canyon floor erosion processes (Shepard, 1981) so is not necessarily contradictory. Divergent and convergent topography in canyon walls due to gullies, however, leads to erosion and accumulation, respectively (e.g., in circled area of Fig. 9b) as sediment creeps off spurs into gullies. This progressively attenuates the gully relief, a tendency that is contradicted by the bathymetry data, which clearly show preserved relief. Therefore, creep may be slower than anticipated (Booth, 1979; Silva and Booth, 1984) or is only a precursor to catastrophic failure (Silva and Booth, 1984), a view compatible with other geotechnical properties of the sediments as water contents are typically above liquid limits and sensitivities (ratio of undisturbed to remoulded shear strength) average 3 (Keller et al., 1979; McGregor et al., 1979). The possibility of diffusive-like topography from creep (Kenyon and Turcotte, 1985) is therefore problematic and would require a uniform and smaller τ_c than implied by the geotechnical test results.

5. Conclusions

Characteristics typical of landscapes that are diffusive-like in the sense used to describe subaerial soil-covered hillslopes have been outlined for various continental slopes and sediment types. For example, the sandy uppermost slope in the Norfolk area is topographically smooth. Hillcrests between canyon heads are convex-upwards and averaged profiles are almost parabolas. In muddy sediment of Monterey Bay, Smooth Ridge has subdued topography and convex-upwards parabolic interfluves occur elsewhere around the bay. Seismic data from the New Jersey slope show patterns of progressive aggradation of interfluves that are similar to those expected if non-deposition along channels acts as a boundary condition to diffusion between the channels. Eel River slope interfluves are parabolic and increase their relief down-slope as expected from channel erosion providing boundary conditions of transport flux increasing downslope.

The gravity effect on saltating sand produces a downslope flux component proportional to bed gradient and thus true diffusion if the residual current effect is comparatively small. Bioturbation requires more investigation but gravity effects on resuspended sediment conceivably also contribute to topographic diffusion. The origins of diffusive-like interfluves of mud, however, are difficult to evaluate with existing data. The growth of the New Jersey slope interfluves, for example, could be explained by accumulation rates decreasing smoothly towards channels because of increasing bed shear stresses from gravity currents and internal waves, an explanation not necessarily compatible with simple diffusion as transport flux may not be down-gradient in direction or proportional to gradient in magnitude. Smooth upwards-convex interfluves could potentially represent levees formed from turbidity current overspill. Creep of clay-rich sediments has been suggested to cause topographic diffusion, but the threshold shear stress for creep more likely leads to abrupt topography associated with threshold gradients of motion.

Effective morphologic modelling using the diffusion equation requires sufficient knowledge of transport process to allow the mobility constant K to be predicted. There is some possibility of this for gravity effects on bedload sand movements and possibly for bioturbation. In order to address the issue of how seabed morphology arises from sediment transport more generally, however, efforts to collect current and suspended and bedload transport data should be expanded from single points as at present to arrays of sites across features such as interfluves. The convergence of derived transport flux could then be compared with Holocene deposition rates to provide insight into morphologic change.

Acknowledgements

We thank the Monterey Bay Aquarium Research Institute and Larry Mayer for generously providing access to multibeam sonar data for Figs. 3 and 5c, the latter funded by the STRATAFORM programme. Grain size data and bathymetry in Fig. 2 were provided by the National Geophysical Data Center (Boulder, Colorado) of the National Oceanographic and Atmospheric Administration, USA. Illustrations were prepared with the Generic Mapping Tools software system (Wessel and Smith, 1991). We thank John Goff, Brian McAdoo, an anonymous reviewer and editor David Piper for their comments which significantly improved this paper. Parts of the paper were written while NCM was on research leave at Scripps Institution of Oceanography, La Jolla, California — NCM thanks his hosts, Steve Cande and others, for their hospitality. NCM was supported by a University Research Fellowship from the Royal Society (London).

Appendix A. Redistribution within the bottom nepheloid layer

Once a suspended sediment concentration anomaly is produced by deposition or erosion, eddy diffusion redistributes suspended sediment to even out the anomaly and allow deposition or erosion to continue. For a water body with no residual current, the equation describing particle diffusion and conservation of mass in the water is:

$$\partial C/\partial t = K_e \partial^2 C/\partial x^2 + v\partial^2 C/\partial z^2 + w_s \partial C/\partial z, \quad \text{(A1)}$$

where C is the suspended sediment concentration (here dimensionless solid volume fraction), K_e and v are lateral and vertical diffusivities (m^2/s) and w_s is particle settling velocity defined earlier. The seabed (at $z=-h$ (m), i.e. h is water depth) alternately experiences erosion and deposition because of unsteady bed stress. Eq. (A1) is used here for only one grain-size component but it can be easily generalised for suspensions of varied grain size. The net change in bed topography caused by erosion at rate E and deposition at rate w_sC is often modelled by

$$\partial h/\partial t = E - w_s C, \quad \text{(A2)}$$

For steady erosion, immediately above the bottom diffusion and erosion will balance, so

$$E = -v\partial C/\partial z. \quad \text{(A3)}$$

The equations can be simplified by representing the variation $C(z)$ with an effective layer thickness derived as follows. Consider a simplified model in which the sediment concentration is steady ($\partial C/\partial t=0$) and laterally uniform ($K\partial^2 C/\partial x^2=0$). A solution to the non-zero elements of Eq. (A1) is then (e.g., Kampf et al., 1999):

$$C = C_0 \exp(-z/D), \quad \text{(A4)}$$

where D is the effective layer thickness equal to v/w_S and C_0 is concentration immediately above the bottom. Now consider a model in which C is steady but not laterally uniform. Integrating Eq. (A1) from the bed up through the bottom layer yields:

$$0 = K_e D \partial^2 C_0/\partial x^2 + E - w_s C_0, \quad \text{(A5)}$$

using Eq. (A3) to replace $\partial C/\partial z$. We define $L \equiv (K_e D/w_S)^{1/2} = (K_e v)^{1/2}/w_S$. The solution of Eq. (A5) is then

$$2Lw_s C_0 = \int_{-\infty}^{x} E(x')\exp[(x'-x)/L]\mathrm{d}x' + \int_{x}^{\infty} E(x')\exp[(x-x')/L]\mathrm{d}x' \quad \text{(A6)}$$

i.e. the sediment concentration is a spatially weighted function of $E(x)$. To illustrate the effect of Eq. (A6), we choose a sinusoidal topography, $H=H_0+H'\sin(kx)$, where k is its spatial frequency, and an erosion rate that is also sinusoidal $E=E_0-E'\sin(kx)$ representing erosion of hills relative to valleys. Evaluating Eq. (A6) for C then yields

$$w_s C = E_0 - E'(1+k^2L^2)^{-1}\sin kx, \quad \text{(A7)}$$

which from Eq. (A2) implies

$$\partial H/\partial t = -E'\sin kx[1+k^{-2}L^{-2}]^{-1} \quad \text{(A8)}$$

The sinusoidal erosion therefore unconditionally reduces seabed relief. Furthermore smaller scales (large k, small […] and largest $[\ldots]^{-1}$) are smoothed fastest. This may explain why the Eel River shelf topography appeared damped (Goff et al., 1999) as eddy diffusion acts most efficiently over short lengthscales.

References

Alexander, C.R., Simoneau, A.M., 1999. Spatial variability in sedimentary processes on the Eel continental slope. Mar. Geol. 154, 243–254.
Allen, P.A., 1997. Earth Surface Processes. Blackwell, Oxford. 404 pp.
Almagor, G., Wiseman, G., 1982. Submarine slumping and mass movements on the continental slope of Israel. In: Saxov, S., Nieuwenhuis, J.K. (Eds.), Marine Slides and Other Mass Movements (NATO Conference Series), vol. 6. Plenum Press, New York, pp. 95–128.
Almagor, G., Bennett, R.H., McGregor, B.A., Shephard, L.E., 1982. Stability studies of surficial sediment in the Wilmington–Lindenkohl Canyons area, eastern U.S. margin. Geo Mar. Lett. 2, 129–134.
Alonso, B., et al., 1985. Morphology of the Ebro Fan valleys from SeaMARC and Sea Beam profiles. Geo Mar. Lett. 5, 141–148.
Anderson, R.S., 1994. Evolution of the Santa Cruz mountains, California, through tectonic growth and geomorphic decay. J. Geophys. Res. 99, 20161–20179.
Anderson, R.F., Bopp, R.F., Buesseler, K.O., Biscaye, P.E., 1988. Mixing of particles and organic constituents in sediments from the continental shelf and slope off Cape Cod: SEEP-I results. Cont. Shelf Res. 8, 925–946.
Anderson, R.F., Rowe, G.T., Kemp, P.F., Trumbore, S., Biscaye, P.E., 1994. Carbon budget for the mid-slope depocentre of the Middle Atlantic Bight. Deep-Sea Res., Part 2, Top. Stud. Oceanogr. 41, 669–703.
Bagnold, R.A., 1963. Mechanics of marine sedimentation. In: Hill, M.N. (Ed.), The Sea, vol. 3. Wiley, New York, pp. 507–528.
Bailard, J.A., Inman, D.L., 1981. An energetics bedload model for a plane sloping beach: local transport. J. Geophys. Res. 86, 2035–2043.
Barry, J.P., et al., 1996. Biologic and geologic characteristics of cold seeps in Monterey Bay, California. Deep-Sea Res., Part 1, Oceanogr. Res. Pap. 43, 1739–1762.
Bennett, R.H., Nelsen, T.A., 1983. Seafloor characteristics and dynamics affecting geotechnical properties at shelfbreaks. In: Stanley, D.J., Moore, G.T. (Eds.), The Shelfbreak: Critical Interface on Continental Margins. Society of Economic Paleontologists and Mineralogists, Tulsa, Oklahoma, pp. 333–355.
Bennett, R.H., Lambert, D.N., Hulbert, M.H., 1977. Geotechnical properties of a sediment slide area on the U.S. continental slope northeast of Wilmington Canyon. Mar. Geotechnol. 2, 245–261.
Booth, J.S., 1979. Recent history of mass-wasting on the upper continental slope, northern Gulf of Mexico, as interpreted from the consolidation states of the sediment. In: Doyle, L.J., Pilkey, O.H.

(Eds.), Geology of Continental Slopes. The Society of Economic Paleontologists and Mineralogists, Tulsa, Oklahoma, pp. 153–164.
Cacchione, D.A., Pratson, L.F., Ogston, A.S., 2002. The shaping of continental slopes by internal tides. Science 296, 724–727.
Carey, J.S., Swift, D.J.P., Steckler, M., Reed, C.W., Niedoroda, A., 1999. High-resolution sequence stratigraphic modeling 2: effects of sedimentation processes, numerical experiments in stratigraphy: recent advances in stratigraphic and sedimentologic computer simulations. SEPM Spec. Publ., vol. 62. SEPM (Society for Sedimentary Geology), pp. 151–164.
Carslaw, H.S., Jaeger, J.C., 1959. Conduction of Heat in Solids. Oxford University Press, Oxford. 510 pp.
Carson, M.A., Petley, D.J., 1970. The existence of threshold hillslopes in the denudation of the landscape. Trans. Inst. Br. Geogr. 49, 71–92.
Casas, D., Ercilla, G., Baraza, J., Alonso, B., Maldonado, A., 2003. Recent mass-movement processes on the Ebro continental slope (NW Mediterranean). Mar. Pet. Geol. 20, 445–457.
Churchill, J.H., Wirick, C.D., Flagg, C.N., Pietrafesa, L.J., 1994. Sediment resuspension over the continental shelf east of the Delmarva Peninsula. Deep-Sea Res., Part 2, Top. Stud. Oceanogr. 41, 341–363.
Clarke, T.L., Swift, D.J.P., Young, R.A., 1983. A stochastic modeling approach to the fine sediment budget of the New York Bight. J. Geophys. Res. 88, 9653–9660.
Collins, C.A., Garfield, N., Rago, T.A., Rischmiller, F.W., Carter, E., 2000. Mean structure of the inshore countercurrent and California undercurrent off Point Sur, California. Deep-Sea Res., Part 2, Top. Stud. Oceanogr. 47, 765–782.
Csanady, G.T., Churchill, J.H., Butman, B., 1988. Near-bottom currents over the continental slope in the Mid-Atlantic Bight. Cont. Shelf Res. 8, 653–671.
Culling, W.E.H., 1960. Analytical theory of erosion. J. Geol. 68, 336–344.
Culling, W.E.H., 1963. Soil creep and the development of hillside slopes. J. Geol. 71, 127–161.
Day, J.H., Field, J.G., Potts Montgomery, M., 1971. The use of numerical methods to determine the distribution of the benthic fauna across the continental shelf of North Carolina. J. Anim. Ecol. 40, 93–125.
Dietrich, W.E., et al., 2003. Geomorphic transport laws for predicting landscape form and dynamics. In: Wilcock, P.R., Iverson, R.M. (Eds.), Prediction in Geomorphology. American Geophysical Union, Washington, D.C., pp. 103–132.
Dillon, W.P., Zimmerman, H.B., 1970. Erosion by biological activity in two New England submarine canyons. J. Sediment. Petrol. 40, 542–547.
Doyle, L.J., Pilkey, O.H., Woo, C.C., 1979. Sedimentation on the eastern United States continental slope. In: Doyle, L.J., Pilkey, O.H. (Eds.), Geology of Continental Slopes. Soc. Econ. Pal. Mineral, Tulsa, Oklahoma, pp. 119–129.
Driscoll, N.W., Karner, G.D., 1999. Three-dimensional quantitative modeling of clinoform development. Mar. Geol. 154, 383–398.
Edwards, B.D., 2002. Variations in sediment texture on the northern Monterey Bay National Marine Sanctuary continental shelf. Mar. Geol. 181, 83–100.
Egbert, G.D., Ray, R.D., Bills, B.G., 2004. Numerical modeling of the global semidiurnal tide in the present day and in the last glacial maximum. J. Geophys. Res. 109 (Art. No. C03003).
Farre, J.A., 1987. Surficial geology of the continental margin offshore New Jersey in the vicinity of Deep Sea Drilling Project Sites 612 and 613. In: Poag, C.W., Watts, A.B. (Eds.), Init. Rep. Deep Sea Drill. Proj., vol. 95. U.S. Gov. Print. Off., Washington, D.C., pp. 725–759.
Field, M.E., Gardner, J.V., Prior, D.B., 1999. Geometry and significance of stacked gullies on the northern California slope. Mar. Geol. 154, 271–286.
Fleming, R.H., 1938. Tides and tidal currents in the Gulf of Panama. J. Mar. Res. 1, 192–206.
Flemings, P.B., Grotzinger, J.P., 1997. STRATA: freeware for analysing clastic stratigraphic problems. GSA Today 6 (12), 1–7.
Flood, R.D., 1988. A lee wave model for deep-sea mudwave activity. Deep-Sea Res. 35, 973–983.
Forde, E.B., Danner Ulrich, S., Hecker, B., 1984. Biological disturbance and camouflage of sedimentary features on the Northeast United States slope and rise. Geo Mar. Lett. 4, 49–53.
Friedrichs, C.T., Wright, L.D., 2004. Gravity-driven sediment transport on the continental shelf: implications for equilibrium profiles near river mouths. Coast. Eng. 51, 795–811.
Gabet, E.J., 2000. Gofer bioturbation: field evidence for non-linear hillslope diffusion. Earth Surf. Process. Landf. 25, 1419–1428.
Gilbert, G.K., 1909. The convexity of hilltops. J. Geol. 17, 344–350.
Goff, J.A., 2001. Quantitative classification of canyon systems on continental slopes and a possible relationship to slope curvature. Geophys. Res. Lett. 28, 4359–4362.
Goff, J.A., Orange, D.L., Mayer, L.A., Hughes Clarke, J.E., 1999. Detailed investigation of continental shelf morphology using a high-resolution swath sonar survey: the Eel margin, northern California. Mar. Geol. 154, 255–269.
Granjeon, D., Joseph, P., 1999. Concepts and applications of a 3-D multiple lithology diffusive model in stratigraphic modeling, numerical experiments in stratigraphy: recent advances in stratigraphic and sedimentologic computer simulations. SEPM Spec. Publ., vol. 62. SEPM (Society for Sedimentary Geology), pp. 197–210.
Green, M.A., Aller, R.C., Cochran, J.K., Lee, C., Aller, J.Y., 2002. Bioturbation in shelf/slope sediments off Cape Hatteras, North Carolina: the use of ^{234}Th, Chl-a, and Br^- to evaluate rates of particle and solute transport. Deep-Sea Res., Part 2, Top. Stud. Oceanogr. 49, 4627–4644.
Greene, H.G., 1977. Geology of the Monterey Bay region. U. S. Geol. Surv. Open-File Rept., vol. 77–718. 347 pp.
Greene, H.G., Maher, N.M., Paull, C.K., 2002. Physiography of the Monterey Bay National Marine Sanctuary and implications about continental margin development. Mar. Geol. 181, 55–82.
Hathaway, J.C., et al., 1976. Preliminary summary of the 1976 Atlantic margin coring project of the U. S. Geological Survey. Open-File Report, vol. 76-844. U. S. Geological Survey.
Hathaway, J.C., et al., 1979. U.S. Geological Survey core drilling on the Atlantic shelf. Science 206, 515–527.
Henderson, G.M., Lindsay, F.N., Slowey, N.C., 1999. Variation in bioturbation with water depth on marine slopes: a study of the Little Bahamas Bank. Mar. Geol. 160, 105–118.
Hill, P.R., Moran, K.M., Blasco, S.M., 1982. Creep deformation of slope sediments in the Canadian Beaufort Sea. Geo Mar. Lett. 2, 163–170.
Howard, A.D., Kerby, G., 1983. Channel changes in badlands. Geol. Soc. Amer. Bull. 94, 739–752.
Huthnance, J.M., 1982a. On one mechanism forming linear sand banks. Estuar. Coast. Shelf Sci. 14, 79–99.
Huthnance, J.M., 1982b. On the formation of sand banks of finite extent. Estuar. Coast. Shelf Sci. 15, 277–299.
Imran, J., Parker, G., Katopodes, N., 1998. A numerical model of channel inception on submarine fans. J. Geophys. Res. 103 (C1), 1219–1238.

Ivanov, V.V., Shapiro, G.I., Huthnance, J.M., Aleynik, D.L., Golovin, P.N., 2004. Cascades of dense water around the world ocean. Prog. Oceanogr. 60, 47–98.

Izumi, N., 2004. The formation of submarine gullies by turbidity currents. J. Geophys. Res. 109, doi:10.1029/2003JC001898 (Paper C03048).

Jordahl, K.A., et al., 2004. Geology of Smooth Ridge: MARS-IODP cabled observatory site. EOS Trans. AGU 85 (47) (Fall Meeting Suppl., Abstract OS43B-0574).

Jordan, T.E., Flemings, P.B., 1991. Large-scale stratigraphic architecture, eustatic variation, and unsteady tectonism: a theoretical evaluation. J. Geophys. Res. 96, 6681–6699.

Kampf, J., Bachaus, J.O., Fohrmann, H., 1999. Sediment-induced slope convection: two-dimensional numerical case studies. J. Geophys. Res. 104, 20509–20522.

Kaufman, P., Grotzinger, J.P., McCormick, D.S., 1991. Depth-dependent diffusion algorithm for simulation of sedimentation in shallow marine depositional systems. In: Franseen, E.K., Watney, W.L., Kendall, C.G.S.C., Ross, W. (Eds.), Sedimentary Modeling: Computer Simulations and Methods for Improved Parameter Definition. Spec. Pub. Kansas Geol. Surv. Bulletin, vol. 233.

Keller, G.E., Shepard, F.S., 1978. Currents and sedimentary processes in submarine canyons off the northeast United States. In: Stanley, D.J., Kelling, G. (Eds.), Sedimentation in Submarine Canyons, Fans, and Trenches. Dowden, Hutchinson & Ross, Pennsylvania, pp. 15–32.

Keller, G.H., Lambert, D.N., Bennett, R.H., 1979. Geotechnical properties of continental slope deposits—Cape Hatteras to Hydrographer Canyon. SEPM Spec. Publ., vol. 27. The Society of Economic Paleontologists and Mineralogists, pp. 131–153.

Kenyon, P.M., Turcotte, D.L., 1985. Morphology of a delta prograding by bulk sediment transport. Bull. Geol. Soc. Am. 96, 1457–1465.

Kirkby, M.J., 1971. Hillslope process — response models based on the continuity equation. Trans. Inst. Br. Geogr., Spec. Publ. 3.

Knebel, H.J., Carson, B., 1979. Small-scale slump deposits, Middle Atlantic continental slope off eastern United States. Mar. Geol. 29, 221–236.

Komar, P.D., 1977. Computer simulation of turbidity current flow and the study of deep-sea channels and fan sedimentation. In: Goldberg, E.D., McCave, I.N., O'Brien, J.J., Steele, J.H. (Eds.), The Sea: Ideas and Observations on Progress in the Study of the Seas. John Wiley & Sons, New York, pp. 603–621.

Krone, R.V., 1976. Engineering interest in the benthic boundary layer. In: McCave, I.N. (Ed.), The Benthic Boundary Layer. Plenum Press, New York, pp. 143–156.

Malahoff, A., Embley, R.W., Perry, R.B., Fefe, C., 1980. Submarine mass-wasting of sediments on the continental slope and upper rise south of Baltimore Canyon. Earth Planet. Sci. Lett. 49, 1–7.

Malahoff, A., Embley, R.W., Fornari, D.J., 1982. Geomorphology of Norfolk and Washington Canyons and the surrounding continental slope and upper rise as observed with DSRV Alvin. In: Scrutton, R.A., Talwani, M. (Eds.), The Ocean Floor. John Wiley and Sons, New York, pp. 97–111.

Masselink, G., Hughes, M.G., 2003. Introduction to Coastal Processes and Geomorphology. Arnold, London. (354 pp.).

MBARI Mapping Team, 2000. Monterey Bay multibeam survey, Monterey Bay Aquarium Research Institute, Digital Data Series No. 3 (CD-ROM).

McCave, I.N., 1984. Erosion, transport and deposition of fine-grained marine sediments. In: Stow, D.A.V., Piper, D.J.W. (Eds.), Fine-grained Sediments: Deep Water Processes and Facies. Blackwell Scientific, Oxford, pp. 35–69.

McCave, I.N., Swift, S.A., 1976. A physical model for the rate of deposition of fine-grained sediments in the deep sea. Geol. Soc. Amer. Bull. 87, 541–546.

McGregor, B.A., 1979. Current meter observations on the U.S. Atlantic continental slope-variation in time and space. Mar. Geol. 29, 209–219.

McGregor, B.A., Bennett, R.H., 1977. Continental slope sediment instability northeast of Wilmington Canyon. Am. Assoc. Pet. Geol. Bull. 61, 918–928.

McGregor, B.A., Bennett, R.H., Lambert, D.N., 1979. Bottom processes, morphology and geotechnical properties of the continental slope south of Baltimore Canyon. Appl. Ocean Res. 1, 177–187.

McHugh, C.M., Ryan, W.B.F., Eittreim, S., Reed, D.L., 1997. The influence of the San Gregorio Fault on the morphology of Monterey Canyon. Mar. Geol. 146, 63–91.

McKean, J.A., Dietrich, W.E., Fenkel, R.C., Southon, J.R., Caffee, M.W., 1993. Quantification of soil production and downslope creep rates from cosmogenic ^{10}Be accumulations on a hillslope profile. Geology 21, 343–346.

Mehta, A.J., Hayter, E.J., Parker, W.R., Krone, R.B., Teeter, A.M., 1989. Cohesive sediment transport: I: process description. J. Hydraul. Eng. 115, 1076–1093.

Middelburg, J.J., Soetaert, K., Herman, P.M.J., 1997. Empirical relationships for use in global diagenetic models. Deep-Sea Res., Part 1, Oceanogr. Res. Pap. 44, 327–344.

Mitchell, N.C., 1995. Diffusion transport model for pelagic sediments on the Mid-Atlantic Ridge. J. Geophys. Res. 100, 19,991–20,009.

Mitchell, N.C., 1996. Creep in pelagic sediments and potential for morphologic dating of marine fault scarps. Geophys. Res. Lett. 23, 483–486.

Mitchell, N.C., 2004. Form of submarine erosion from confluences in Atlantic USA continental slope canyons. Am. J. Sci. 304, 590–611.

Mitchell, N.C., 2005. Interpreting long-profiles of canyons in the USA Atlantic continental slope. Mar. Geol. 214, 75–99.

Mitchell, N.C., 2006. Morphologies of knickpoints in submarine canyons. Geol. Soc. Amer. Bull. 118, 589–605.

Nagel, D.K., Mullins, H.T., Greene, H.G., 1986. Ascension submarine canyon, California — evolution of a multi-head canyon system along a strike–slip continental margin. Mar. Geol. 73, 285–310.

Nelsen, T.A., Bennett, R.H., 1981. Signatures of surficial sand and small-scale mass wasting of sediments at shelf break and upper slope seaward of Baltimore Canyon Trough. Am. Assoc. Pet. Geol. Bull. 65, 1667–1668.

Niedoroda, A.M., Reed, C.W., Swift, D.J.P., Arata, H., Hoyanagi, K., 1995. Modeling shore-normal large-scale coastal evolution. Mar. Geol. 126, 181–199.

Orange, D.L., et al., 1999. Widespread fluid expulsion on a translational continental margin: mud volcanoes, fault zones, headless canyons, and organic-rich substrate in Monterey Bay, California. Geol. Soc. Amer. Bull. 111, 992–1009.

Parchure, T.M., Mehta, A.J., 1985. Erosion of soft cohesive sediment deposits. J. Hydraul. Eng., ASCE 111, 1308–1326.

Parker, G., Fukushima, Y., Pantin, H.M., 1986. Self-accelerating turbidity currents. J. Fluid Mech. 171, 145–181.

Paull, C.K., Mitts, P., Ussler, W., Keaten, R., Greene, H.G., 2005a. Trail of sand in upper Monterey Canyon: offshore California. Geol. Soc. Amer. Bull. 117, 1134–1145.

Paull, C.K., Ussler, W., Greene, H.G., Barry, J., Keaten, R., 2005b. Bioerosion by chemosynthetic biological communities on Holocene submarine slide scars. Geo Mar. Lett. 25, 11–19.

Penn, B.S., Harbaugh, J.W., 1999. The role of positive feedback in the development of interval oscillations for a simple, tightly coupled, nearshore depositional model, numerical experiments in stratigraphy: recent advances in stratigraphic and sedimentologic computer simulations. SEPM Spec. Publ., vol. 62. SEPM (Society for Sedimentary Geology), pp. 265–270.

Perkins, R.G., Paterson, D.M., Sun, H., Watson, J., Player, M.A., 2004. Extracellular polymeric substances: quantification and use in erosion experiments. Cont. Shelf Res. 24, 1623–1635.

Pietrafesa, L.J., 1983. Shelfbreak circulation, fronts and physical oceanography: east and west coast persepectives. In: Stanley, D.J., Moore, G.T. (Eds.), The Shelfbreak: Critical Interface on Continental Margins. Society of Economic Paleontologists and Mineralogists, Tulsa, Oklahoma, pp. 233–250.

Pratson, L.F., Ryan, W.B.F., Mountain, G.S., Twichell, D.C., 1994. Submarine canyon initiation by downslope-eroding sediment flows: evidence in late Cenozoic strata on the New Jersey continental slope. Geol. Soc. Amer. Bull. 106, 395–412.

Queney, P., 1948. The problem of air flow over mountains: a summary of theoretical studies. Bull. Am. Meteorol. Soc. 29, 16–26.

Quiquerez, A., Allemand, P., Dromart, G., Garcia, J.-P., 2004. Impact of storms on mixed carbonate and silliclastic shelves: insights from combined diffusive and fluid flow transport stratigraphic forward model. Basin Res. 16, 431–449.

Ramp, S.R., Abbott, C.L., 1998. The vertical structure of currents over the continental shelf off Point Sur, CA, during spring 1990. Deep-Sea Res., Part 2, Top. Stud. Oceanogr. 45, 1443–1470.

Rivenaes, J.C., 1992. Application of a dual-lithology, depth dependent diffusion equation in stratigraphic simulation. Basin Res. 4, 133–146.

Rivenaes, J.C., 1997. Impact of sediment transport efficiency on large-scale sequence architecture: results from stratigraphic computer simulation. Basin Res. 9, 91–105.

Robb, J.M., Hampson, J.C., Kirby, J.R., Twichell, D.C., 1981a. Geology and potential hazards of the continental slope between Lindenkohl and South Toms Canyons, offshore Mid-Atlantic United States. U. S. Geol. Surv. Open-File Rept, 81–600. 33pp.

Robb, J.M., Hampson, J.C., Twichell, D.C., 1981b. Geomorphology and sediment stability of a segment of the U.S. continental slope off New Jersey. Science 211, 935–937.

Roering, J.J., Kirchner, J.W., Dietrich, W.E., 1999. Evidence for nonlinear, diffusive sediment transport on hillslopes and implications for landscape morphology. Water Resour. Res. 35, 853–870.

Sawyer, W.B., Ransom, B., Bennett, R.H., 1997. Geotechnical property variability of continental margin sediments: high-resolution vertical and lateral data from the northern California slope. Mar. Georesour. Geotechnol. 15, 283–304.

Schlager, W., Adams, E.W., 2001. Model for the sigmoidal curvature of submarine slopes. Geology 29, 883–886.

Schlee, J., et al., 1976. Regional geologic framework off Northeastern United States. Am. Assoc. Pet. Geol. Bull. 60, 926–951.

Schmidt, S., van Weering, T.C.E., Reyss, J.-L., van Beek, P., 2002. Seasonal deposition and reworking at the sediment–water interface on the northwestern Iberian margin. Prog. Oceanogr. 52, 331–348.

Scully, M.E., Friedrichs, C.T., Wright, L.D., 2002. Application of an analytical model of critically stratified gravity-driven sediment transport and deposition to observations from the Eel River continental shelf, Northern California. Cont. Shelf Res. 22, 1951–1974.

Selby, M.J., 1993. Hillslope Materials and Processes. Oxford University Press, Oxford. 451 pp.

Shapiro, G.I., Huthnance, J.M., Ivanov, V.V., 2003. Dense water cascading off the continental shelf. J. Geophys. Res. 108, doi:10.1029/2002JC001610.

Shepard, F.S., 1979. Currents in submarine canyons and other seavalleys. SEPM Spec. Publ., vol. 27. The Society of Economic Paleontologists and Mineralogists, pp. 85–94.

Shepard, F.P., 1981. Submarine canyons: multiple causes and long-time persistence. Bull. Am. Assoc. Pet. Geol. 65, 1062–1077.

Silva, A.J., Booth, J.S., 1984. Creep behavior of submarine sediments. Geo Mar. Lett. 4, 215–219.

Small, E.E., Anderson, R.S., Hancock, G.S., 1999. Estimates of the rate of regolith production using Be-10 and Al-26 from an alpine hillslope. Geomorphology 27, 131–150.

Smith, C.R., Levin, L.A., Hoover, D.J., McMurtry, G., Gage, J.D., 2000. Variations in bioturbation across the oxygen minimum zone in northwest Arabian Sea. Deep-Sea Res. 47, 227–257.

Soetaert, K., et al., 1996. Modelling ^{210}Pb-derived mixing activity in ocean margin sediments: diffusive versus nonlocal mixing. J. Mar. Res. 54, 1207–1227.

Southard, J.B., Stanley, D.J., 1976. Shelf-break processes and sedimentation. In: Stanley, D.J., Swift, D.J.P. (Eds.), Marine Sediment Transport and Environmental Management. John Wiley & Sons, New York, pp. 351–377.

Spinelli, G.A., Field, M.E., 2001. Evolution of continental slope gullies on the Northern California Margin. J. Sediment. Res. 71, 237–245.

Spinelli, G.A., Field, M.E., 2003. Controls of tectonics and sediment source locations on along-strike variations in transgressive deposits on the northern California Margin. Mar. Geol. 197, 35–47.

Stanley, D.J., 1971. Fish-produced markings on the outer continental margin east of the middle Atlantic states. J. Sediment. Petrol. 41, 159–170.

Stanley, D.J., Wear, C.M., 1978. The “mud-line:” an erosion-deposition boundary in the upper continental slope. Mar. Geol. 28, M19–M29.

Stanley, D.J., Addy, S.K., Behrens, E.W., 1983. The mudline: variability of its position relative to shelfbreak. In: Stanley, D.J., Moore, G.T. (Eds.), The Shelfbreak: Critical Interface on Continental Margins. Society of Economic Paleontologists and Mineralogists, Tulsa, Oklahoma, pp. 279–298.

Syvitski, J.P.M., Daughney, S., 1992. DELTA2: Delta progradation and basin filling. Comput. Geosci. 18, 839–897.

Syvitski, J.P.M., Smith, J.N., Calabrese, E.A., Boudreau, B.P., 1988. Basin sedimentation and the growth of prograding deltas. J. Geophys. Res. 93, 6895–6908.

Ter Stepanian, G., 1975. Creep of clay during shear and its rheological model. Geotechnique 25, 299–320.

Tucker, G.E., Bras, R.L., 1998. Hillslope processes, drainage density, and landscape morphology. Water Resour. Res. 34, 2751–2764.

Valentine, P.C., Uzmann, J.R., Cooper, R.A., 1980. Geologic and biologic observations in Oceanographer submarine canyon: descriptions of dives aboard the research submarsibles Alvin (1967, 1978) and Nekton Gamma (1974). U.S. Geological Survey Open File Report, vol. 80-76. 40pp.

van Asch, T.W.J., van Genuchten, P.M.B., 1990. A comparison between theoretical and measured creep profiles of landslides. Geomorphology 3, 45–55.

van Asch, T.W.J., Deimel, M.S., Haak, W.J.C., Simon, J., 1989. The viscous creep component in shallow clayey soil and the influence of tree load on creep rates. Earth Surf. Process. Landf. 14, 557–564.

Warme, J.E., Slater, R.A., Cooper, R.A., 1978. Bioerosion in submarine canyons. In: Stanley, D.J., Kelling, G. (Eds.), Sedimentation in Submarine Canyons, Fans, and Trenches. Dowden, Hutchinson & Ross, Stroudsburg, pp. 65–70.

Weatherly, G.L., 1993. On deep-current and hydrographic observations from a mudwave region and elsewhere in the Argentine Basin. Deep-Sea Res., Part 2, Top. Stud. Oceanogr. 40, 939–961.

Webb, H.F., Jordan, T.H., 1993. Quantifying the distribution and transport of pelagic sediments on young abyssal hills. Geophys. Res. Lett. 20, 2203–2206.

Webb, H.F., Jordan, T.H., 2001a. Pelagic sedimentation on rough seafloor topography. 1. Forward model. J. Geophys. Res. 106, 30,433–30,449.

Webb, H.F., Jordan, T.H., 2001b. Pelagic sedimentation on rough seafloor topography. 2. Inversion results from the North Atlantic acoustic reverberation corridor. J. Geophys. Res. 106, 30,451–30,473.

Wessel, P., Smith, W.H.F., 1991. Free software helps map and display data. EOS Trans. AGU 72, 441.

Wheatcroft, R.A., 1991. Conservative tracer study of horizontal sediment mixing rates in a bathyal basin, California Borderland. J. Mar. Res. 49, 565–588.

Wheatcroft, R.A., Jumars, P.A., Smith, C.R., Nowell, A.R.M., 1990. A mechanistic view of the particulate biodiffusion coefficient: step length, rest periods and transport directions. J. Mar. Res. 48, 177–207.

Wolfe, C.J., McNutt, M.K., Detrick, R.S., 1994. The Marquesas archipelagic apron: seismic stratigraphy and implications for volcano growth, mass wasting, and underplating. J. Geophys. Res. 99, 13591–13608.

Wright, L.D., Friedrichs, C.T., Kim, S.C., Scully, M.E., 2001. Effects of ambient currents and waves on gravity-driven sediment transport on continental shelves. Mar. Geol. 175, 25–45.

Wright, L.D., Friedrichs, C.T., Scully, M.E., 2002. Pulsational gravity-driven sediment transport on two energetic shelves. Cont. Shelf Res. 22, 2443–2460.